Durable Light-Driven pH Switch for CO_2 Capture/Release Enabled by Tuning Solvation Environment of Photoacids

Anna de Vries[a], Kateryna Goloviznina[b], Manuel Reiter[a], Mathieu Salanne[b,c], Maria R. Lukatskaya[a*]

[a] Electrochemical Energy Systems Laboratory, Department of Mechanical and Process Engineering, ETH Zurich, 8092 Zurich, Switzerland

[b] Sorbonne Université, CNRS, Physico-Chimie des Électrolytes et Nanosystèmes Interfaciaux, PHENIX, F-75005 Paris, France

[c] Institut Universitaire de France (IUF), 75231 Paris, France

* Corresponding author email: mlukatskaya@ethz.ch

ABSTRACT: Photoacids are organic molecules that release protons under illumination, providing spatiotemporal control of pH. Such light-driven pH switches offer the ability to cyclically alter the pH of the medium and are highly attractive for a wide variety of applications, including CO_2 capture. Although photoacids such as protonated merocyanine can enable fully reversible pH cycling in water, they have a limited chemical stability against hydrolysis (<24 hours). Moreover, these photoacids have low solubility and provide only a small pH-jump. In this work we introduce a simple pathway to dramatically increase stability and solubility of photoacids by tuning their solvation environment in binary solvent mixtures. We show that a preferential solvation of merocyanine by aprotic solvent molecules results in a 60% increase in pH modulation magnitude when compared to the behavior in pure water and can withstand stable cycling for > 350 hours. Our results suggest that a very high stability of merocyanine photoacids can be achieved in the right solvent mixtures, offering a way to bypass complex structural modifications of photoacid molecules and serving as the key milestone towards their application in a photo-driven CO_2 capture process.

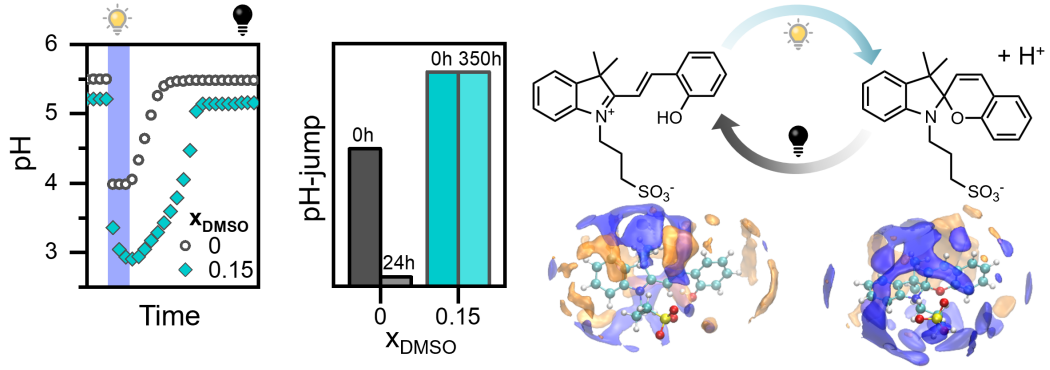

KEYWORDS: solvent mixtures · photoacids · molecular switches · solvation environment · stability · CO_2 capture

INTRODUCTION

Proton transfer plays a fundamental role in regulating (electro)chemical processes relevant for catalysis[1-3], energy[4] and CO_2 storage[5,6] and many others.[7-10] Therefore, noninvasive external control of the pH is highly desirable for modulation of proton-coupled (electro)chemical reactions and equilibria. A unique class of molecules that are capable of generating H^+ *on demand* upon illumination are called photoacids. Photoacids are organic molecules that possess higher acidity in their light-induced excited state compared to their ground state in darkness.[1] The proton-transfer for these compounds is highly reversible: photoacids release a proton to their environment under excitation by UV or visible light, while in darkness, they return to the ground state by thermal relaxation and recombining with a proton. Metastable photoacids (mPAHs) are a subclass of photoacids that can alter the pH of a solution through proton release as a result of photoisomerization. Such a mechanism allows mPAHs to remain in their deprotonated state for 9-10 orders of magnitude longer than other types of photoacids[11]. The relaxation at the order of seconds-minutes makes it possible for released protons to diffuse away from their counterions and can thus reversibly alter the bulk pH in a solution.[1,12] For example, protonated merocyanine (MCH) photoacids, the archetype of mPAHs, undergo *trans*-to-*cis* isomerization under UV-Vis illumination - leading to a proton release, followed by a ring-closing reaction to spiropyran (SP) (**Scheme 1**).[1,12,13] As a result, bulk solution pH can drop by several units within seconds and return to initial pH in darkness within minutes.[1,12,14,15]. As mPAHs provide remote pH-control of the medium, achievable by a moderate intensity of visible light, they have been demonstrated numerous applications[16,17], among them are: functionalized surfaces, such as membranes[18] and sensors[19]; acid-catalyzed reactions such as drug delivery[20,21], volume-change of hydrogels[12,22]; controlling physicochemical properties of polymers such as conductivity with light[23,24]; reversible nano-assembly of DNA[25] and molecular machines[26,27].

Recently, there has been a growing interest in employing photoacids for CO_2 capture applications.[28-30] This approach harnesses a photo-driven pH change, offering an attractive alternative to the energy-intensive pressure and temperature swings that are traditionally used for sorbent regeneration.[31] In the process that employs photoacids, CO_2 is first captured by an alkaline solution (sorbent) containing protonated photoacid, leading to the formation of bicarbonate (HCO_3^-).[32-34] Next, to regenerate, the sorbent solution is exposed to light, triggering the release of protons followed by bicarbonate protonation, which in turn releases gaseous CO_2.[28] Finally, in the dark, the photoacid reverts to its protonated state, leading to an overall increase in pH and thereby regenerating the sorbent, completing the capture-release cycle (**Scheme 1**).

However, these practical applications of photoacids are challenged by insufficient stability of mPAH in aqueous media and limited solubility.[35-37] In water, more than half of MCH undergoes hydrolysis along the bridging C=C bond within the first 24 hours.[35] Meanwhile, low solubility constraints the magnitude of the pH drop, especially for solutions that are buffered, such as in CO_2 capture applications.[38] Main efforts to improve the chemical stability and solubility were focused on modifying the chemical structure of merocyanine by adding electron donating and withdrawing substituents to the conjugated system.[14-16,39,40] Other approaches include post-synthesis modifications such as confinement of photoacid molecules into coordination cages.[41-43] While with these approaches the chemical half-life can be

improved from 16 hours up to several days[35], for real applications, such as CO_2 capture, it is necessary to demonstrate a long-term cycling stability.[44] However, to the best of our knowledge, demonstration of prolonged light cycling stability with such molecular approaches are still limited to a maximum of 17 hours of operation.[25] Stability of photoacids is known to be affected by solvent environment[1,13], where higher stability can be achieved in non-aqueous solutions (e.g. methanol[40,45-47], DMF[47], DMSO[40,47-49]). In aprotic solvents, higher stability is enabled by natural suppression of the degradation pathway through hydrolysis.[13] However, the proton release of the photoacids is practically irreversible in aprotic solvents in contrast to protic ones.[1,48,50] To enable reversible pH change with photoacids, solvents or solvent mixtures with extended H-bonding network are necessary to facilitate proton transfer back to the photoacid in the darkness.[50]

In this work, we probe stability and solubility of photoacids in water-DMSO mixtures. DMSO was selected as a cosolvent because it offers at least two orders of magnitude higher photoacid solubility and solubility compared to water[13]. Further, in water-DMSO mixtures freezing occurs at much lower temperatures (down to -140 °C).[51,52] As efficiency of MCH pH-switching scales inversely with temperature[53], incorporation of photoacids in water-DMSO mixtures would enable improved magnitude and temperature range of such pH switches[53]. Additionally, low toxicity[54] and vapor pressure (0.051 kPa)[55] of DMSO are particularly beneficial for long term operation that is necessary in continuous processes such as CO_2 capture.[56-58]

Herein, we show that merocyanine-type photoacids in water-DMSO solvent mixtures can achieve both high reversibility of the proton release as well as high chemical stability and solubility. We have selected a classical protonated merocyanine photoacid in water-DMSO mixtures as a model system as it is the most-studied structure.[12,35] We demonstrate that solubility and pH modulation under illumination can be enhanced by one order of magnitude in solvent mixtures compared to pure water. Furthermore, we show that the stability of MCH can be dramatically extended in the solvent mixtures, prolonging pH cycling for over 350 hours. By means of classical molecular dynamics (MD) simulations with polarizable force fields, we reveal the crucial role of the photoacid solvation environment in the observed enhancements. Finally, as a proof-of-concept, we show that a co-solvent approach can also be applied to benefit light-driven CO_2 release.

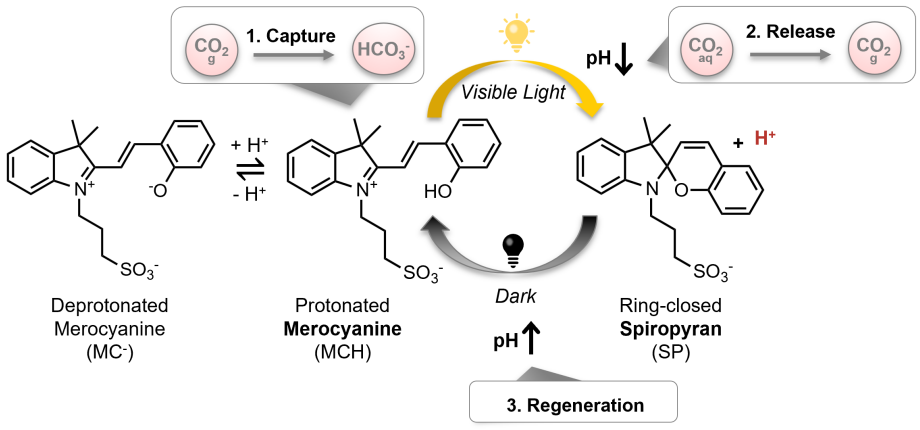

Scheme 1. Simplified photochemistry of protonated merocyanine photoacid and 3-step process of light-driven CO_2 capture-release.

RESULTS AND DISCUSSION

Photo-switching behavior of merocyanine photoacid in water-DMSO mixtures

To analyze the role of DMSO on photoacid properties, we first characterized the pH-jump, ΔpH, and reversibility time, t_{rev} (**Figure 1**). The pH-jump (**Equation 1**) is the difference between the solution pH when the photoacid is in the ground state in darkness (pH^{GS}) and in the metastable state during illumination (pH^{MS}). The reversibility time (t_{rev}) is the time it takes for the solution pH to return to the initial pH^{GS} upon thermal relaxation.

$$\Delta pH = pH^{GS} - pH^{MS} \qquad \textit{Equation 1}$$

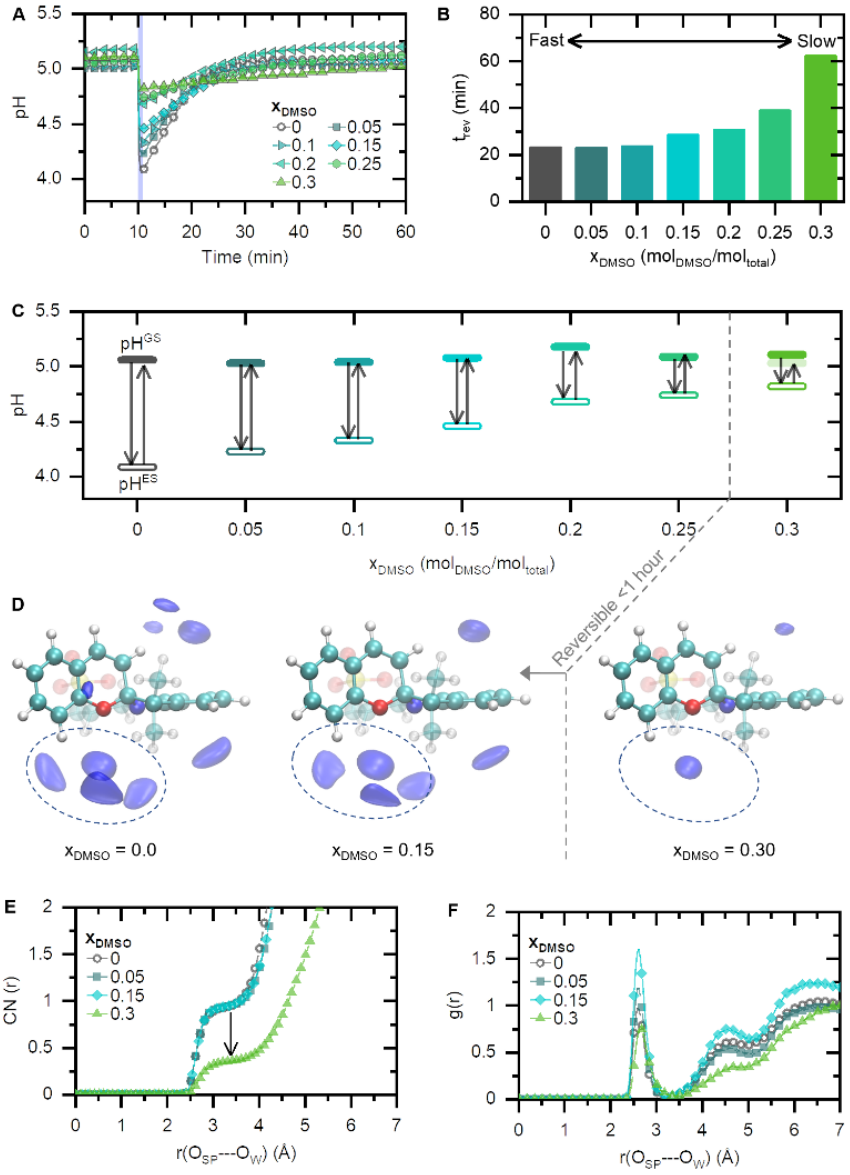

Figure 1. (A) pH-jump after illumination (at t = 10 min) of 0.08 mM $mPAH_{tot}$ at different DMSO mole fractions (x_{DMSO}), **(B)** reversibility time upon relaxation to MCH in darkness, and **(C)** pH-jump as a function of x_{DMSO}, where the dotted line indicates that at $x_{DMSO} \geq 0.3$ the original pH cannot be recovered within 1 hour of darkness. **(D)** Spatial distribution functions of oxygen atoms of water (blue isosurface) around SP molecule cut at the absolute density of 95 nm^{-3}. **(E)** Coordination numbers of oxygen atoms of water around the oxygen atom of the SP molecule and **(F)** radial distribution functions of oxygen atoms of water around the oxygen atom of the SP molecule.

For these measurements, solutions with equal photoacid concentrations (0.08 mM) were prepared (preparation details in Methods). As shown in **Figures 1A-C**, in pure water a pH-jump of 0.8 units is observed. However, an increase in DMSO fraction leads to a decrease in the magnitude and efficiency of the pH-jump (**Figures 1A-C**). At x_{DMSO} = 0.3 the pH-jump is limited to 0.3 units due to low proton release efficiency of 7.3%. Similarly, the time for the pH to reverse to the original pH^{GS} (t_{rev}) gradually increases as a function of x_{DMSO} (**Figures 1 A, B**) and at $x_{DMSO} \geq 0.3$ the pH-jump is no longer fully reversible within 1 hour (since for applications the fast pH modulation is desired[1,16,35,59], only t_{rev} up to 1 hour was considered). It is important to note that the proton release efficiency and reversibility time can be significantly affected by the setup (e.g. light power, wavelength, path-length, stirring efficiency) and results therefore may differ between reports[13]. Also, due to the change in activity coefficients and liquid junction potentials in the presence of non-aqueous solvents, the pH values in different solvent mixtures should be treated as trends rather than absolute values.[60-62] If absolute pH values across different solvent compositions are required, they can be obtained following the procedures by Radtke and Heering et al.[63,64]

We used MD simulations to understand the impact of different solvent ratios in water-DMSO mixtures on the reversibility of the proton transfer to spiropyran (ring-closed form that is reached in the metastable state, **Scheme 1**). The structure can be analyzed through the calculation of radial distribution functions, which measure the probability of finding atoms at a particular distance around a central reference atom, and from which coordination numbers can be derived. Our results, shown in **Figures 1E, F**, indicate that the solvation environment of spiropyran changes notably as the DMSO content increases. In particular, the fraction of water molecules coordinating with the oxygen atom of spiropyran drops significantly at higher DMSO concentrations, from 0.94 ($x_{DMSO} \leq 0.15$) down to 0.35 at higher DMSO content (x_{DMSO} = 0.3). This behavior is also reflected in the radial distribution functions: the intensity of the first peak initially increases with lowering water content (dilution effect), but dramatically decreases once x_{DMSO} = 0.3 is achieved (**Figure 1F**). Similarly, at x_{DMSO} = 0.3 we observe a diminishment of the second solvation of water (formed at ~5.1 Å) visible from spatial distribution functions (**Figure 1D**) and leading to the coordination number decrease by a factor of three (from 5.0 at x_{DMSO} = 0.15 to 1.5 at x_{DMSO} = 0.3), which shows the absence of water nanocluster in the vicinity of the oxygen atom of spiropyran. These changes in the solvation environment limit the possibility of passing protons through the hydrogen bonding network of water to spiropyran, blocking the ring-opening reaction (SP → MC^-, **Scheme 1**).

Enhanced chemical stability by solvation environment tuning

Next, we studied the chemical stability of MCH in water-DMSO mixtures. The degradation happens via a nucleophilic attack of water to the bridging C=C bond, leading to formation of salicylaldehyde (D1) and 2,3,3-trimethyl-1-(4-sulfobutyl)-indolium (D2), as shown in **Figure 2A**.[35] For x_{DMSO} = 0, 0.15 and 1, using ^{1}H-NMR we tracked evolution of the peaks corresponding to MCH and products of its hydrolysis over a course of 12 weeks (**Figure 2B**). In water, the photoacid hydrolyzes rapidly: peaks from D2 (singlet peak at ~1.6 ppm denoted as *c**, $(CH_3)_2$-groups) are already present in the as-prepared sample (0 days) and the intensity increases sharply within the first 24 hours. Concurrently, a steady decrease in intensity is observed for peaks corresponding to $(CH_3)_2$- groups of equilibrium forms of unhydrolyzed photoacid: MCH/MC^- (~1.85 ppm, singlet, c) and SP (~1.2 and ~1.3 ppm, doublet, c'). Analysis of the hydrolysis rates in water reveals that half of the mPAH is degraded within 1 day (**Figure 2C**). In contrast, in 100% DMSO no degradation products were detected even after 12 weeks: integrals for $(CH_3)_2$-groups of MCH/MC^- at

~1.77 ppm remain stable over time, while the SP form is not observed (absence of the doublet at < 1.4 ppm in **Figure 2B**). Meanwhile, in the mixture of both solvents (x_{DMSO} = 0.15) the hydrolysis is significantly suppressed (**Figure 2C**) with half of the photoacid concentration still present after 20 days.

Using MD simulations, this enhanced stability of merocyanine in water-DMSO mixtures compared to pure water can be explained from a structural point of view: in the first coordination shell of the bridging double bond of MCH, water molecules are progressively replaced by DMSO nanodomains with an increase in DMSO content, as shown in **Figure 2F**. In particular, we observe higher coordination numbers for DMSO and lower ones for water than expected from the ideal mixing (dashed line in **Figure 2D**).

This excess of DMSO points to the preferable solvation of the double bond by the organic solvent. As a result, at x_{DMSO} = 0.3, the coordination number of the oxygen atom of DMSO reaches 65 % of the maximum value in pure DMSO, preventing water species from approaching and reacting with the double bond. In the hydrolysis mechanism, the phenol/phenolate fragment of MCH plays an important role: Andréasson *et al.*[37] showed that the phenolate oxygen (O^-) of MC^- coordinates the water molecule approaching the bridging double bond, favoring water dissociation, and the O^- then stabilizes the formed proton.

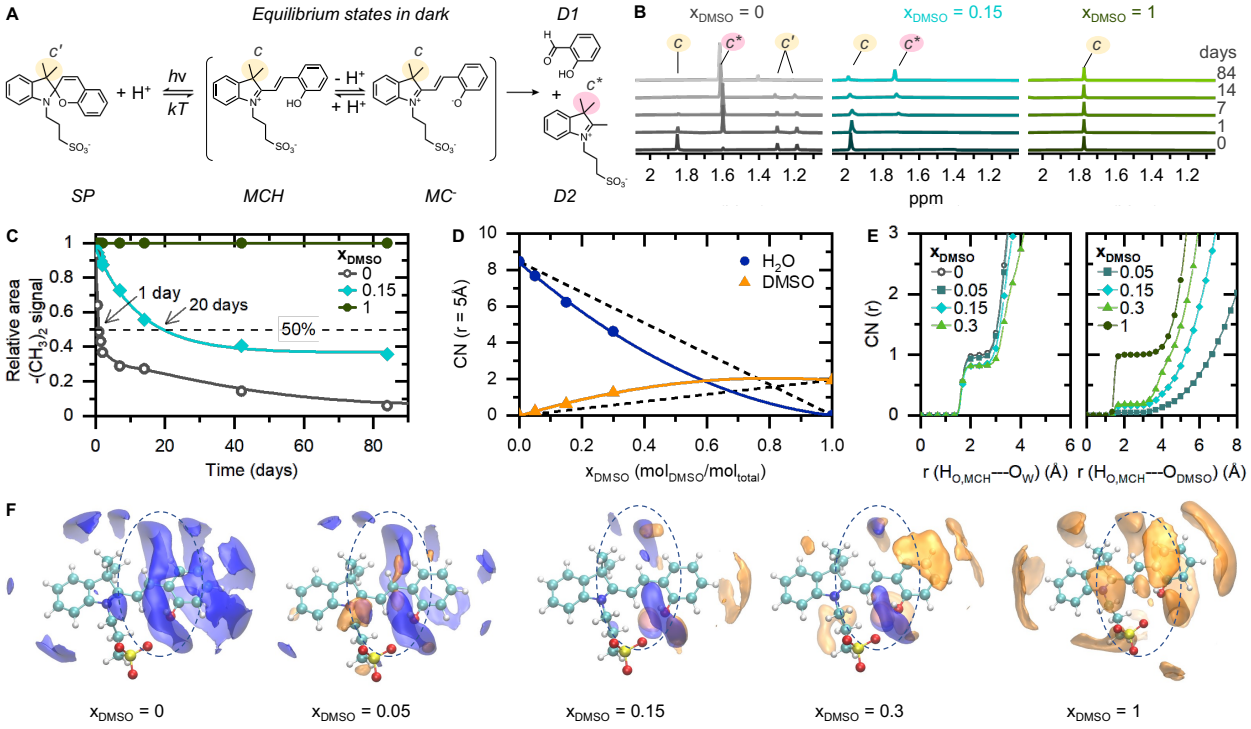

Figure 2. (A) Schematic of the equilibrium between ring closed spiropyran (SP), protonated- and deprotonated merocyanine (MCH and MC^- respectively), and degradation products salicylaldehyde (D1) and indolium (D2). **(B)** ^{1}H-NMR spectra of $mPAH_{tot}$ in D_2O (0.2 mM), $x_{d\text{-}DMSO}$ = 0.15 (5.3 mM) and d_6-DMSO (17.5 mM). **(C)** Chemical degradation over 12 weeks obtained from ^{1}H-NMR signals. **(D)** Coordination numbers of oxygen atoms of water (blue) and DMSO (orange) around the double bond of the MCH molecule, evaluated at a distance of 5 Å, as a function of DMSO mole fraction. **(E)** Coordination numbers of oxygen atoms of water (left) and DMSO (right) around hydrogen atom of the hydroxyl group of the MCH molecule. **(F)** Spatial distribution functions of oxygen atoms of water (blue isosurface) and DMSO (orange isosurface) around the MCH molecule. Isosurfaces are cut at the absolute density of 60 nm^{-3} for water and 4.5, 7.5, 13 and 14 nm^{-3} for x_{DMSO} = 0.05, 0.15, 0.30 and 1, respectively.

While the addition of water to the non-dissociated OH group of MCH requires overcoming a significantly higher energy barrier, making this reaction path less probable. Formation of the metastable MC^- anion from the stable MCH form requires the proximity of water molecules to the phenol moiety. The presence of DMSO can perturb the H-bonding network, hampering the proton transfer from the solute to the solvent. MD simulations show that with the increase of the DMSO content, the coordination number of oxygen atoms of water around the hydroxyl group of MCH (measured at ~2.35 Å from H atom) decreases from 1.0 (x_{DMSO} = 0) to0.82 (x_{DMSO} = 0.15) and remains almost unchanged up to x_{DMSO} = 0.3. Water molecules are replaced by those of DMSO since the inverse trend in coordination numbers is observed for oxygen atoms of DMSO (**Figure 2E**). Even though only 0.18 O_{DMSO} (x_{DMSO} = 0.15) can be found around the OH group, it seems to be already sufficient to hinder the dissociation of the MCH, consequently stabilizing MCH in the solution.

Optimizing solubility and stability for long term operation

Degradation of the mPAH can be further accelerated with illumination: repeated illumination or photoisomerization can lead to photobleaching.[65] So far, photochemical stability has only been reported in water for MC-type photoacids up to 17 hours of total operation.[25,35] To probe the photochemical stability, we measured the pH of the photoacid solutions under light modulation (1 minute light, 58 minutes dark, full procedure can be found in Methods). As can be seen in **Figure 3A-B**, the photochemical stability follows the same trend as chemical, as it increases with DMSO fraction: solutions at x_{DMSO}= 0.25 lost only 32% of the pH-jump magnitude after 150 hours of cycling in contrast to the case of pure water, where 53% was already lost after 24 hours. Faster degradation was observed for the solutions that were subject to light cycling compared to those kept in darkness (**Figure 3C** and Supplementary Information S3).

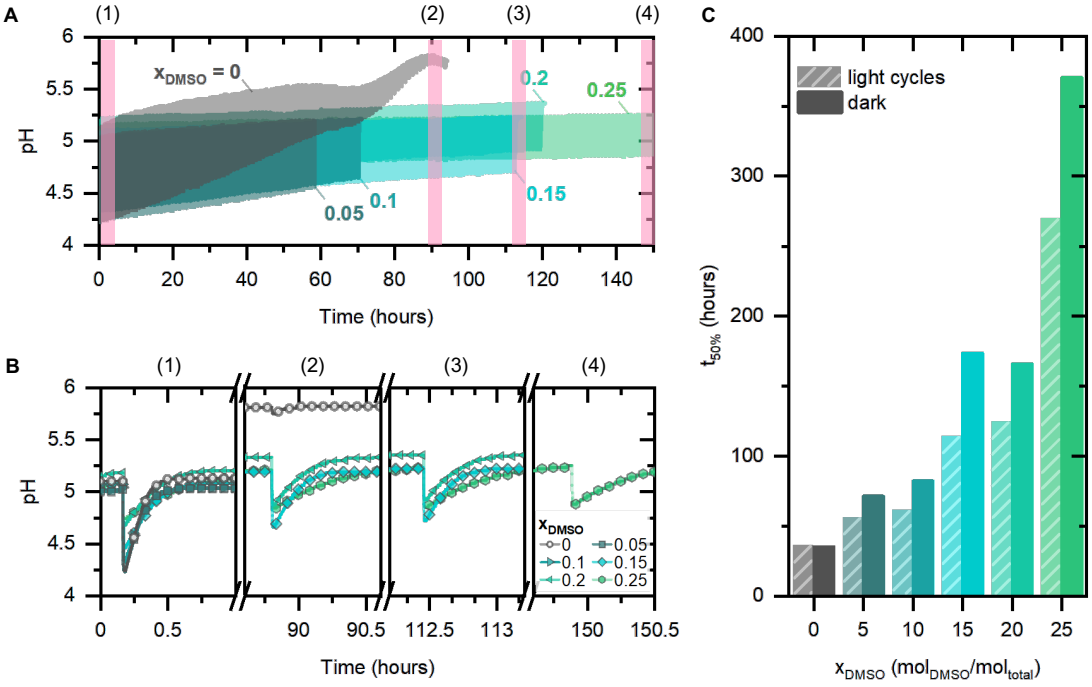

Figure 3. (A) Photochemical stability upon light cycles of 0.08 mM $mPAH_{ot}$ at different x_{DMSO} where data is shown until 50% proton release degradation, with the exception of x_{DMSO} = 0 and 0.25 for which data is shown until 99% and 35% degradation respectively. **(B)** pH-jump corresponding to selected regions in (A) at 0 (1), 90 (2), 113 (3) and 150 (4) hours. **(C)** Time at which half of the protons are released during pH-jump compared to the first cycle ($t_{50\%}$).

Despite a notable improvement in chemical and photochemical stability of photoacid in water-DMSO mixtures (**Figures 2, 3**), for the same concentration of mPAH smaller pH-jumps with higher x_{DMSO} (**Figure 1A, C**). In water, an increase in mPAH concentration leads to higher pH-jumps because more photoacid is present to release protons (Supplementary Figure S9). Meanwhile, we show that in water-DMSO mixtures an order of magnitude enhanced solubility can be achieved (**Figure 4A**, Table S2). Our computational results (**Figure 1D**) show that H_2O primarily solvates polar regions and DMSO solvates non-polar regions. Subsequently, we characterized pH-jumps for saturated MCH solutions at different x_{DMSO} values. Similar to the case of water, higher mPAH solubility led to a proportional increase in pH-jumps upon illumination (**Figure 4B,** Supplementary Figure S10). Thanks to enhanced solubility, the highest pH-jump in saturated conditions was reached in x_{DMSO} = 0.15 with 2.4 units, whereas in pure water the pH-jump reached 1.5 units (**Figures 4B**).

Next, we evaluated the long-term light cycling stability (**Figure 4C**, Supplementary Information S4) of a saturated photoacid solution (5.3 mM) in x_{DMSO} = 0.15 – the sample for which the highest pH-jump is reached. Dissolving the photoacid in x_{DMSO} = 0.15 allows for significant improvements in stability: at least 2 weeks of stable light cycles is achieved with a lasting pH-jump that is higher than in pure water (**Figure 4C**).

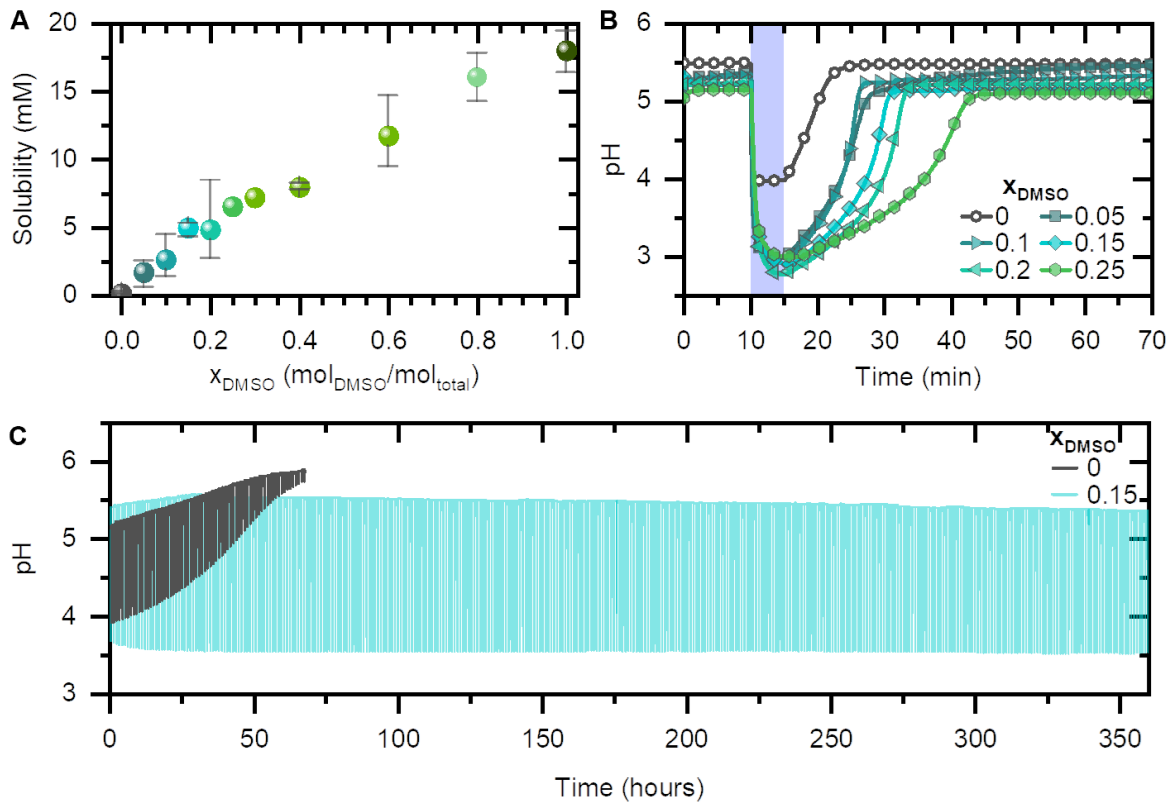

Figure 4. **(A)** Solubility curve of merocyanine photoacid in water-DMSO mixtures and **(B)** pH change after illumination of saturated mPAH (at t = 10 min) at different x_{DMSO}. **(C)** Long term stability of 0.2 mM $mPAH_{tot}$ in water and 5.3 mM in x_{DMSO} = 0.15, cycling by 1 minute light and 58 minutes darkness.

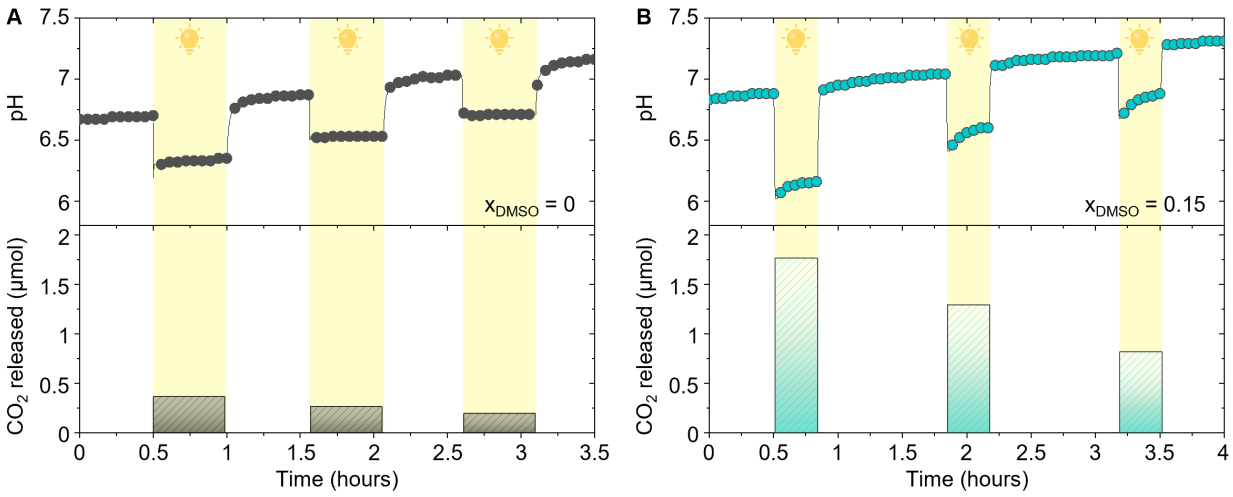

Figure 5. pH change (top) and cumulative CO_2 release (bottom) from a solution with 0.2 mM $mPAH_{tot}$ and 0.2 mM $KHCO_3$ in pure H_2O **(A)**, and 5.3 mM $mPAH_{tot}$ and 5.3 mM $KHCO_3$ x_{DMSO} = 0.15 **(B)** while cycling between light (yellow highlight) and dark.

Finally, as a proof-of-concept, we demonstrate the feasibility of using MCH in water-DMSO mixtures for light-driven CO_2 capture-release (**Figure 5**). For this, CO_2 was introduced by adding $KHCO_3$ to the mixture at the ratio of $KHCO_3$:MCH = 1:1 to mitigate the buffering effect of $KHCO_3$ (Supplementary Information S6). As a result, a pH-jump could trigger a substantial release of CO_2. Because the DMSO co-solvent enables much higher concentrations of the dissolved photoacid (0.2 mM in water vs. 5.3 mM in x_{DMSO} = 0.15), we could use a higher $KHCO_3$ concentration (given the aforementioned 1:1 ratio). Upon illumination, five times more CO_2 was released in the water-DMSO mixture compared to water. After each consecutive illumination cycle, the amount of released CO_2 gradually decreases (**Figure 5**). Given the enhanced stability and solubility of the merocyanine photoacid in water-DMSO mixtures (Figure 4), this demonstration serves as a steppingstone for enabling a stable light-driven CO_2 capture-release.

CONCLUSIONS

We show that an enhanced stability and solubility of photoacids can be achieved when a simple water-DMSO mixture is used as a solvent. Up to x_{DMSO} = 0.25, the solution containing merocyanine returns to its initial pH within 1 hour after illumination. We show that the chemical stability of the photoacid in water-based solutions containing DMSO can be extended by a factor of 20 (compared to pure water) under light cycling conditions. At x_{DMSO} = 0.15, a reversible pH-jump of up to 2.4 units can be achieved due to an enhanced solubility of merocyanine in the presence of DMSO. Using molecular dynamics simulations, we explain these results by the changes in the solvation environment of the photoacid. Our work shows that the use of binary solvent mixtures such as water-DMSO offers a simple way to optimize a pH-jump, solubility, and (photo)chemical stability of photoacids. We anticipate that the stability of other photoacids that are susceptible to hydrolysis can be dramatically improved in binary solvent mixtures due to their preferential solvation by aprotic solvent molecules. Finally, our work demonstrates that higher amounts of light-driven CO_2 capture-release (relative to water) can be achieved for photoacids stabilized through the right solvation environment.

METHODS

General

All chemicals were purchased from Sigma Aldrich, TCI Chemicals, VWR International or Chemie Brunschwig AG and used without further purification. To avoid variations in degree of degradation, solutions were always freshly prepared before experiments and/or analysis unless noted otherwise. UV-Vis absorption spectra were collected using an Agilent *Cary 5000* or Perkin Elmer *Lambda 35*. The spectra were measured in 70 µl UV-microcuvettes (BRAND®), unless specified otherwise. The pH was measured using Mettler Toledo pH electrodes *LE438* (polyester junction, 12 mm diameter) or *LE422* (ceramic junction, 4.3 mm diameter). pH data was recorded using an Oakton *pH 700 Benchtop Meter* and logged every 3 seconds by the *CyberComm 2700* computer software. Nuclear Magnetic Resonance (NMR) spectra were measured on a Bruker 400 MHz spectrometer. For NMR measurements, D_2O (99.9%, Chemie Brunschwig AG) or d_6-DMSO (99.9%, Sigma Aldrich) solvents were used for sample preparation. Chemical shifts were referenced to residual ^1H signals of the solvent. In pH-jump measurements and photochemical degradation studies, photoacids were illuminated using a 405 nm LED (*M405L4*, 14 mW/cm^2, Thorlabs), controlled by an LED driver (*LEDD1B*, Thorlabs). Light modulation cycles were programmed using a waveform generator (*DG1022z*, Rigol).

Synthesis

Synthesis and characterization are provided in the Supplementary Information.

pH-jump and reversibility

To ensure that all solutions have a similar starting pH of 5.25 ± 0.2, 2 vials containing basic and acidic solutions of the photoacid were prepared in the respective solvent mixture (described below). First, appropriate amounts of the photoacid were dissolved in DMSO (99.9%, VWR International AG). Next, to each vial, an aqueous solution of 10 mM NaOH or HCl was added to achieve the targeted water-DMSO ratio. To ensure an optimal response of the pH electrode, 20 mM NaCl was added to photoacid solutions. Finally, acidic and basic solutions were titrated to reach the target pH. To avoid light exposure, solutions were always kept in polypropylene vials (CELLSTAR® Greiner Bio-One), wrapped in aluminum foil. The pH-jump and reversibility were measured in a 2 x 2 x 2 cm quartz cuvette (Portmann Instruments). For each measurement, 6 mL of photoacid solution was used and continuously stirred with a 5 mm Teflon stirring bar, rotating at 200 rpm. The cuvette was placed in a custom-made optical cell, which had a 18 x 18 mm window for light exposure of 1 or 5 minutes (405 nm LED, M405L4, 14 mW/cm2, Thorlabs) and an airtight lid holding the pH electrode.

Prior to each experiment, the pH electrodes were calibrated by a 3-point calibration with technical buffer standards (pH 4, 7, 10). To minimize the drift effect due to different solvent compositions inside pH-electrode and measured liquid, prior to each measurement the pH electrode was stabilized in the respective solvent mixture for 20 minutes. It is important to note, that while with such pH measurement approach we followed the manufacturer recommendation of measurements in organic solvents[66], the obtained results do not account for possible differences of the liquid junction potentials (LJP). LJP can be different in solvent mixtures compared to pure water[60,61], and therefore can affect the readings of the pH meter[62].

Therefore, the pH values in different solvent mixtures should be treated as trends rather than absolute values.

Chemical stability

To study the chemical stability of MCH in different solvents, we prepared the following solutions: 0.2 mM in D_2O, 5.3 mM in $x_{d6\text{-}DMSO}$ = 0.15 and 17.5 mM in pure d_6-DMSO. The samples were measured using amber NMR tubes (5 mm, Norell™) that prior to each use were cleaned with water, acetone, and deuterated solvent and dried in a vacuum oven. Assignment of the characteristic peaks (a, b', c, c') was done in accordance with a prior study by Berton et al.[13] We tracked the degradation of the photoacid samples using positions of the $(CH_3)_2$ singlet NMR peaks, denoted as c, c*, or c' (Figure 2, Supplementary Figure S4). We also measured a reference spectrum of salicylaldehyde (D1) in D_2O to reference the position of the d*. All data was processed and analyzed using the MestReNova software. We monitored the samples over 12 weeks.

Photochemical stability

To evaluate the photochemical stability, the photoacid solutions were subjected to the following light modulation cycles using a 405 nm LED (*M405L4*, 14 mW/cm^2, Thorlabs): 1 minute light on and 58 minutes light off for dilute samples (Figure 3A). To calculate the degradation percentage, we compared the released effective proton concentration estimated from the pH-jump with cycling to the amount measured for the first cycle (Equation 2). $t_{50\%}$ is the time at which 50% of degradation is reached (Figure 3C). In other words, $t_{50\%}$ is the time at which only half of the protons is released during pH-jump compared to the first cycle (Equation 3).

$$Degradation\ (\%) = \frac{10^{-pH_{t_0}} - 10^{-pH_{t_x}}}{10^{-pH_{t_0}}} * 100\% \qquad \textit{Equation 2}$$

$$t_{50\%}(hours) = 50 * \frac{t_x\ (hours)}{Degradation_{t_x}(\%)} \qquad \textit{Equation 3}$$

To compare the chemical and photochemical degradation, an additional 6 mL of each solution was stored in a vial in the dark for the duration of the light cycle experiment. At the end of the light cycle measurements, we performed a single pH-jump measurement of this sample (Supplementary Figures S5, 3C).

Solubility

Due to different solvation properties of water and DMSO of the merocyanine molecule, we wanted to study whether different solubilities can be achieved depending on the preparation procedure. Step-by-step procedure is provided in Supplementary Information S5.

Simulation methodology

Molecular dynamics simulations of periodic cubic boxes were performed in OpenMM software[67]. Each system contained one solute molecule (merocyanine or spiropyran) placed at the center of a box and surrounded by a sufficient quantity of solvent to approximate infinite dilution. The total number of solvent molecules was set to 2000, and the molar fractions of DMSO, x_{DMSO} = 0, 0.05, 0.15. 0.3, and 1 were considered. Initial configurations were generated using PACKMOL[68], and the input files were prepared with fftool[69] and polarizer[70] utilities. A cut-off of 12 Å was set for non-bonded interactions, with the tail correction applied for energy and pressure. Particle Mesh Ewald (PME) method was used to evaluate electrostatic energies, with a tolerance of 10^{-5}. Bonds involving hydrogen atoms and the H-O-H angle of water

were constrained using SHAKE algorithm. A time step of 1 fs was considered. Dual Langevin thermostat and Monte Carlo barostat were applied for temperature and pressure control, with the values set to 298 K and 1 bar, respectively. The systems were equilibrated for 5 ns in the NPT ensemble, and then 100 ns trajectories were generated in the NVT ensemble.

Drude induced dipoles were used to represent explicit polarization effects.[71] Each site consisted of a positively charged Drude core (DC) with a negatively charged Drude particle (DP) of a mass of 0.4 a.u., attached to the core with a harmonic spring (k_D = 4184 kJ/mol). The maximum elongation of the spring was constrained to 0.05 Å in order to prevent a "polarization catastrophe".[72] Partial charges of the DPs were evaluated from atomic polarizabilities, $q_D = \sqrt{\alpha k_D}$. Only non-hydrogen atoms were treated as polarizable, with atomic polarizability of hydrogen atoms summed onto the polarizability of the atoms to which they are attached. Thole damping function[73] with the universal parameter of 2.6 [74] was used to smear short-range interactions between the induced dipoles. The relative motion of DPs with respect to their cores was regulated at a temperature of 1 K as an approximation of the self-consistent regime.[71]

Water (W) was modelled using the existing SWM4-NDP polarizable force field.[75] Polarizable models of merocyanine (MCH) and spiropyran (SP) were developed following the CL&Pol approach,[76,77] while the force field for DMSO was already published earlier.[76] The atomic partial charges of the solutes (Supplementary Table S4) were evaluated using CHelpG methodology[78] at MP2/cc-pVTZ level at previously optimized geometries in Gaussian[79]. Bonded and non-bonded Lennard-Jones interaction parameters were taken from OPLS-AA force field.[80] Atomic polarizabilities were adapted from the work of Schröder.[81] Initial well-depths (ε_{ij}) of Lennard-Jones potential were modified in order to remove double counting of polarization effects,[76] already represented by Drude induced dipoles. Water-water interaction parameters were not modified and the interactions of water with other species were scaled only partially since the water model was already polarizable.[77] Following the assumption of infinite dilution, solute-solute interactions were not modified either. All the molecules/ions were considered as entire fragments. The scaling factors (k_{ij}), evaluated using the predictive scheme,[76] are given in Supplementary Table S5. The atomic diameters (σ) were kept unchanged.

TRAVIS[82,83] software was used for the structure analysis of the trajectories, and the spatial distribution functions (SDF) were visualized in VMD.[84] The reference *xy* plane passes through C2, N1, and C3 atoms for SDFs of SP, and though C10, C11, and C12 atoms for SDFs around the double C=C bond of MCH.

SUPPLEMENTARY INFORMATION

Supplementary Information contains synthetic and experimental procedures, supplementary calculations, and simulation methodology.

AUTHOR CONTRIBUTIONS

Conceptualization, A.D.V. and M.R.L.; Methodology, A.D.V., K.G., M.R., M.S. and M.R.L.; Investigation, A.D.V., K.G., M.R., M.S. and M.R.L..; Writing – Original Draft, A.D.V. K.G. and M.R.L.; Writing – Review & Editing, A.D.V., K.G., M.R., M.S. and M.R.L.; Visualization, A.D.V., K.G. and M.R.L.; Funding Acquisition, M.S. and M.R.L.; Resources, M.S. and M.R.L.; Supervision, M.S. and M.R.L.

DECLARATION OF INTEREST

The authors declare no competing interests.

ACKNOWLEDGMENTS

A.D.V. thanks Dr. Bruno Marco-Dufort for his advice on optimizing synthetic procedures and scientific discussions. M.R.L. acknowledges support from ReMaP project funded by the Swiss Federal Office of Energy under contract SI/501810-01 and the ETH Foundation. K.G. and M.S. acknowledge the funding from European Research Council (ERC) under the European Union's Horizon 2020 research and innovation program (grant agreement 771294). MD simulations were performed using resources from GENCI-IDRIS (grants 2021-A0100910463 and 2022-A0120910463).

REFERENCES

(1) Liao, Y. Design and Applications of Metastable-State Photoacids. Acc. Chem. Res. 2017, 50, 1956-1964.

(2) Nunes, R. M. D.; Pineiro, M.; Arnaut, L. G. Photoacid for Extremely Long-Lived and Reversible pH-Jumps. Journal of the American Chemical Society 2009, 131, 9456-9462.

(3) Ghorbani-Choghamarani, A.; Taherinia, Z. Recent advances utilized in artificial switchable catalysis. RSC Advances 2022, 12, 23595-23617.

(4) Derr, J. B.; Tamayo, J.; Clark, J. A.; Morales, M.; Mayther, M. F.; Espinoza, E. M.; Rybicka-Jasinska, K.; Vullev, V. I. Multifaceted aspects of charge transfer. Phys Chem Chem Phys 2020, 22, 21583-21629.

(5) Millero, F. J. Thermodynamics of the carbon dioxide system in the oceans. Geochimica et Cosmochimica Acta 1995, 59, 661-677.

(6) Orr, J. C.; Fabry, V. J.; Aumont, O.; Bopp, L.; Doney, S. C.; Feely, R. A.; Gnanadesikan, A.; Gruber, N.; Ishida, A.; Joos, F.; Key, R. M.; Lindsay, K.; Maier-Reimer, E.; Matear, R.; Monfray, P.; Mouchet, A.; Najjar, R. G.; Plattner, G.-K.; Rodgers, K. B.; Sabine, C. L.; Sarmiento, J. L.; Schlitzer, R.; Slater, R. D.; Totterdell, I. J.; Weirig, M.-F.; Yamanaka, Y.; Yool, A. Anthropogenic ocean acidification over the twenty-first century and its impact on calcifying organisms. Nature 2005, 437, 681-686.

(7) Liao, Y. Reversible photo control of proton chemistry. Physical Chemistry Chemical Physics 2022, 24, 4116-4124.

(8) Kohse, S.; Neubauer, A.; Pazidis, A.; Lochbrunner, S.; Kragl, U. Photoswitching of Enzyme Activity by Laser-Induced pH-Jump. Journal of the American Chemical Society 2013, 135, 9407-9411.

(9) Luo, Y.; Wang, C.; Peng, P.; Hossain, M.; Jiang, T.; Fu, W.; Liao, Y.; Su, M. Visible light mediated killing of multidrug-resistant bacteria using photoacids. Journal of Materials Chemistry B 2013, 1, 997-1001.

(10) Wang, L.; Li, Q. Photochromism into nanosystems: towards lighting up the future nanoworld. Chemical Society Reviews 2018, 47, 1044-1097.

(11) Tolbert, M. L.; Solntsev, M. K. Excited state Proton Transfer From Constrained Systems to super photoacids to superfast proton transfer. Acc. Chem. Res. 2002, 35, 19-27.

(12) Shi, Z.; Peng, P.; Strohecker, D.; Liao, Y. Long-lived photoacid based upon a photochromic reaction. J. Am. Chem. Soc. 2011, 133, 14699-14703.

(13) Berton, C.; Busiello, D. M.; Zamuner, S.; Solari, E.; Scopelliti, R.; Fadaei-Tirani, F.; Severin, K.; Pezzato, C. Thermodynamics and kinetics of protonated merocyanine photoacids in water. Chem. Sci. 2020, 11, 8457-8468.

(14) Liu, J.; Tang, W.; Sheng, L.; Du, Z.; Zhang, T.; Su, X.; Zhang, S. X. Effects of Substituents on Metastable-State Photoacids: Design, Synthesis, and Evaluation of their Photochemical Properties. Chem. Asian J. 2019, 14, 438-445.

(15) Berton, C.; Busiello, D. M.; Zamuner, S.; Scopelliti, R.; Fadaei-Tirani, F.; Severin, K.; Pezzato, C. Light-Switchable Buffers. Angew. Chem. Int. Ed. 2021, 60, 21737-21740.

(16) Wimberger, L.; Prasad, S. K. K.; Peeks, M. D.; Andreasson, J.; Schmidt, T. W.; Beves, J. E. Large, Tunable, and Reversible pH Changes by Merocyanine Photoacids. J. Am. Chem. Soc. 2021, 143, 20758-20768.
(17) Kozlenko, A. S.; Ozhogin, I. V.; Pugachev, A. D.; Lukyanova, M. B.; El-Sewify, I. M.; Lukyanov, B. S. A Modern Look at Spiropyrans: From Single Molecules to Smart Materials. Topics in Current Chemistry 2023, 381, 8.
(18) White, W.; Sanborn, C. D.; Fabian, D. M.; Ardo, S. Conversion of Visible Light into Ionic Power Using Photoacid-Dye-Sensitized Bipolar Ion-Exchange Membranes. Joule 2018, 2, 94-109.
(19) Johns, V. K.; Patel, P. K.; Hassett, S.; Calvo-Marzal, P.; Qin, Y.; Chumbimuni-Torres, K. Y. Visible light activated ion sensing using a photoacid polymer for calcium detection. Anal. Chem. 2014, 86, 6184-6187.
(20) Han, R.; Wu, S.; Tang, K.; Hou, Y. Facilitating drug release in mesoporous silica coated upconversion nanoparticles by photoacid assistance upon near-infrared irradiation. Advanced Powder Technology 2020, 31, 3860-3866.
(21) Fagan, A.; Bartkowski, M.; Giordani, S. Spiropyran-Based Drug Delivery Systems. Frontiers in Chemistry 2021, 9.
(22) Meeks, A.; Lerch, M. M.; Schroeder, T. B. H.; Shastri, A.; Aizenberg, J. Spiropyran Photoisomerization Dynamics in Multiresponsive Hydrogels. J. Am. Chem. Soc. 2022, 144, 219-227.
(23) Imato, K.; Momota, K.; Kaneda, N.; Imae, I.; Ooyama, Y. Photoswitchable Adhesives of Spiropyran Polymers. Chem. Mater. 2022, 34, 8289-8296.
(24) Keyvan Rad, J.; Balzade, Z.; Mahdavian, A. R. Spiropyran-based advanced photoswitchable materials: A fascinating pathway to the future stimuli-responsive devices. J. Photochem. Photobiol. C 2022, 51, 100487.
(25) Wimberger, L.; Rizzuto, F. J.; Beves, J. E. Modulating the Lifetime of DNA Motifs Using Visible Light and Small Molecules. Journal of the American Chemical Society 2023, 145, 2088-2092.
(26) Silvi, S.; Arduini, A.; Pochini, A.; Secchi, A.; Tomasulo, M.; Raymo, F. M.; Baroncini, M.; Credi, A. A Simple Molecular Machine Operated by Photoinduced Proton Transfer. Journal of the American Chemical Society 2007, 129, 13378-13379.
(27) Baroncini, M.; Silvi, S.; Credi, A. Photo- and Redox-Driven Artificial Molecular Motors. Chemical Reviews 2020, 120, 200-268.
(28) Bennett, R.; Clifford, S.; Anderson, K.; Puxty, G. Carbon Capture Powered by Solar Energy. Energy Procedia 2017, 114, 1-6.
(29) Premadasa, U. I.; Bocharova, V.; Miles, A. R.; Stamberga, D.; Belony, S.; Bryantsev, V. S.; Elgattar, A.; Liao, Y.; Damron, J. T.; Kidder, M. K.; Doughty, B.; Custelcean, R.; Ma, Y.-Z. Photochemically-Driven CO2 Release Using a Metastable-State Photoacid for Energy Efficient Direct Air Capture. Angewandte Chemie International Edition 2023, n/a, e202304957.
(30) Alghazwat, O.; Elgattar, A.; Liao, Y. Photoacid for releasing carbon dioxide from sorbent. Photochemical & Photobiological Sciences 2023.
(31) Deutz, S.; Bardow, A. Life-cycle assessment of an industrial direct air capture process based on temperature–vacuum swing adsorption. Nature Energy 2021, 6, 203-213.
(32) Wang, X.; Conway, W.; Burns, R.; McCann, N.; Maeder, M. Comprehensive Study of the Hydration and Dehydration Reactions of Carbon Dioxide in Aqueous Solution. The Journal of Physical Chemistry A 2010, 114, 1734-1740.
(33) Bülow, M.; Gerek Ince, N.; Hirohama, S.; Sadowski, G.; Held, C. Predicting Vapor–Liquid Equilibria for Sour-Gas Absorption in Aqueous Mixtures of Chemical and Physical Solvents or Ionic Liquids with ePC-SAFT. Industrial & Engineering Chemistry Research 2021, 60, 6327-6336.

(34) Zeebe, R. E.; Wolf-Gladrow, D.: CO2 in Seawater: Equilibrium, Kinetics, Isotopes; Elsevier Science, 2001.
(35) Abeyrathna, N.; Liao, Y. Stability of merocyanine-type photoacids in aqueous solutions. J. Phys. Org. Chem. 2017, 30.
(36) Stafforst, T.; Hilvert, D. Kinetic characterization of spiropyrans in aqueous media. Chem. Commun. 2009, 287-288.
(37) Hammarson, M.; Nilsson, J. R.; Li, S.; Beke-Somfai, T.; Andreasson, J. Characterization of the thermal and photoinduced reactions of photochromic spiropyrans in aqueous solution. J. Phys. Chem. B 2013, 117, 13561-13571.
(38) Abeyrathna, N.; Liao, Y. A Reversible Photoacid Functioning in PBS Buffer under Visible Light. J. Am. Chem. Soc. 2015, 137, 11282-11284.
(39) Wimberger, L.; Andreasson, J.; Beves, J. E. Basic-to-acidic reversible pH switching with a merocyanine photoacid. Chem. Commun. 2022, 58, 5610-5613.
(40) Zayas, M. S.; Dolinski, N. D.; Self, J. L.; Abdilla, A.; Hawker, C. J.; Bates, C. M.; Read de Alaniz, J. Tuning Merocyanine Photoacid Structure to Enhance Solubility and Temporal Control: Application in Ring Opening Polymerization. ChemPhotoChem 2019, 3, 467-472.
(41) Samanta, D.; Galaktionova, D.; Gemen, J.; Shimon, L. J. W.; Diskin-Posner, Y.; Avram, L.; Král, P.; Klajn, R. Reversible chromism of spiropyran in the cavity of a flexible coordination cage. Nature Communications 2018, 9, 641.
(42) Wang, J.; Avram, L.; Diskin-Posner, Y.; Białek, M. J.; Stawski, W.; Feller, M.; Klajn, R. Altering the Properties of Spiropyran Switches Using Coordination Cages with Different Symmetries. Journal of the American Chemical Society 2022, 144, 21244-21254.
(43) Miskolczy, Z.; Biczók, L. Photochromism in Cucurbit[8]uril Cavity: Inhibition of Hydrolysis and Modification of the Rate of Merocyanine–Spiropyran Transformations. The Journal of Physical Chemistry B 2011, 115, 12577-12583.
(44) Diederichsen, K. M.; Sharifian, R.; Kang, J. S.; Liu, Y.; Kim, S.; Gallant, B. M.; Vermaas, D.; Hatton, T. A. Electrochemical methods for carbon dioxide separations. Nat. Rev. Dis. Primers 2022, 2.
(45) Tatum, L. A.; Foy, J. T.; Aprahamian, I. Waste Management of Chemically Activated Switches: Using a Photoacid To Eliminate Accumulation of Side Products. Journal of the American Chemical Society 2014, 136, 17438-17441.
(46) Alghazwat, O.; Elgattar, A.; Khalil, T.; Wang, Z.; Liao, Y. Red-light responsive metastable-state photoacid. Dyes and Pigments 2019, 171, 107719.
(47) Joseph, P.; Kundu, K.; Kundu, P. K. Merocyanines of Non-Activated Spiropyrans: Generation and Spectrokinetic Studies. ChemistrySelect 2018, 3, 11065-11070.
(48) Johns, V. K.; Wang, Z.; Li, X.; Liao, Y. Physicochemical study of a metastable-state photoacid. J. Phys. Chem. A 2013, 117, 13101-13104.
(49) Aldaz, C. R.; Wiley, T. E.; Miller, N. A.; Abeyrathna, N.; Liao, Y.; Zimmerman, P. M.; Sension, R. J. Experimental and Theoretical Characterization of Ultrafast Water-Soluble Photochromic Photoacids. The Journal of Physical Chemistry B 2021, 125, 4120-4131.
(50) Pines, D.; Pines, E.: Solvent Assisted Photoacidity. In Hydrogen-Transfer Reactions, 2006; pp 377-415.
(51) Venkatraman, R. K.; Baiz, C. R. Ultrafast Dynamics at the Lipid-Water Interface: DMSO Modulates H-Bond Lifetimes. Langmuir 2020, 36, 6502-6511.
(52) Kirchner, B.; Reiher, M. The Secret of Dimethyl Sulfoxide-Water Mixtures. A Quantum Chemical Study of 1DMSO-nWater Clusters. J Am Chem Soc 2002, 124, 6206-6215.
(53) Périllat, V. J.; Berton, C.; Pezzato, C. The effect of temperature on the photoacidity of merocyanine photoacids in water. Materials Today Chemistry 2022, 25, 100918.

(54) Gironi, B.; Kahveci, Z.; McGill, B.; Lechner, B.-D.; Pagliara, S.; Metz, J.; Morresi, A.; Palombo, F.; Sassi, P.; Petrov, P. G. Effect of DMSO on the Mechanical and Structural Properties of Model and Biological Membranes. Biophysical Journal 2020, 119, 274-286.
(55) Qian, X.; Han, B.; Liu, Y.; Yan, H.; Liu, R. Vapor pressure of dimethyl sulfoxide and water binary system. Journal of Solution Chemistry 1995, 24, 1183-1189.
(56) Zhou, X.; Liu, C.; Fan, Y.; Zhang, L.; Tang, S.; Mo, S.; Zhu, Y.; Zhu, Z. Energy-efficient carbon dioxide capture using a novel low-viscous secondary amine-based nonaqueous biphasic solvent: Performance, mechanism, and thermodynamics. Energy 2022, 255, 124570.
(57) Zhou, X.; Li, X.; Wei, J.; Fan, Y.; Liao, L.; Wang, H. Novel Nonaqueous Liquid–Liquid Biphasic Solvent for Energy-Efficient Carbon Dioxide Capture with Low Corrosivity. Environmental Science & Technology 2020, 54, 16138-16146.
(58) Li, X.; Zhou, X.; Wei, J.; Fan, Y.; Liao, L.; Wang, H. Reducing the energy penalty and corrosion of carbon dioxide capture using a novel nonaqueous monoethanolamine-based biphasic solvent. Separation and Purification Technology 2021, 265, 118481.
(59) Kagel, H.; Frohme, M.; Glökler, J. Photoacids in biochemical applications. J. Cell. Biotechnol. 2019, 4, 23-30.
(60) Izutsu, K. Liquid Junction Potentials between Electrolyte Solutions in Different Solvents. Analytical Sciences 2011, 27, 685-694.
(61) Senanayake, G.; Muir, D. M. Studies on the liquid junction potential corrections of electrolytes at aqueous + mixed solvent boundaries. Journal of Electroanalytical Chemistry and Interfacial Electrochemistry 1987, 237, 149-162.
(62) Dunsmore, H. S.; Midgley, D. The calibration of glass electrodes in cells with liquid junction. Analytica Chimica Acta 1972, 61, 115-122.
(63) Heering, A.; Stoica, D.; Camões, F.; Anes, B.; Nagy, D.; Nagyné Szilágyi, Z.; Quendera, R.; Ribeiro, L.; Bastkowski, F.; Born, R.; Nerut, J.; Saame, J.; Lainela, S.; Liv, L.; Uysal, E.; Roziková, M.; Vičarová, M.; Snedden, A.; Deleebeeck, L.; Radtke, V.; Krossing, I.; Leito, I. Symmetric Potentiometric Cells for the Measurement of Unified pH Values. Symmetry [Online early access]. DOI: 10.3390/sym120711502020.
(64) Radtke, V.; Stoica, D.; Leito, I.; Camões, F.; Krossing, I.; Anes, B.; Roziková, M.; Deleebeeck, L.; Veltzé, S.; Näykki, T.; Bastkowski, F.; Heering, A.; Dániel, N.; Quendera, R.; Liv, L.; Uysal, E.; Lawrence, N. A unified pH scale for all solvents: part I – intention and reasoning (IUPAC Technical Report). 2021, 93, 1049-1060.
(65) Demchenko, A. P. Photobleaching of organic fluorophores: quantitative characterization, mechanisms, protection*. Methods Appl. Fluoresc. 2020, 8, 022001.
(66) Measurement in Organic Solvents. https://www.mt.com/ca/en/home/library/applications/lab-analytical-instruments/measurement-pH-organic-solvents.html 2023).
(67) Eastman, P.; Swails, J.; Chodera, J. D.; McGibbon, R. T.; Zhao, Y.; Beauchamp, K. A.; Wang, L.-P.; Simmonett, A. C.; Harrigan, M. P.; Stern, C. D.; Wiewiora, R. P.; Brooks, B. R.; Pande, V. S. OpenMM 7: Rapid development of high performance algorithms for molecular dynamics. PLoS Comput. Biol. 2017, 13, e1005659.
(68) Martínez, L.; Andrade, R.; Birgin, E. G.; Martínez, J. M. PACKMOL: A package for building initial configurations for molecular dynamics simulations. J. Comput. Chem. 2009, 30, 2157-2164.
(69) Padua, A.: fftool. 2022.
(70) Goloviznina, K.; Padua, A.: polarizer. 2022.
(71) Lamoureux, G.; Roux, B. T. Modeling induced polarization with classical Drude oscillators: Theory and molecular dynamics simulation algorithm. Chem. Phys. 2003, 119, 3025-3039.

(72) Huang, J.; Lemkul, J. A.; Eastman, P. K.; Mackerell, A. D. Molecular dynamics simulations using the drude polarizable force field on GPUs with OpenMM: Implementation, validation, and benchmarks. J. Comput. Chem. 2018, 39, 1682-1689.
(73) Thole, B. T. Molecular polarizabilities calculated with a modified dipole interaction. Chem. Phys. 1981, 59, 341-350.
(74) Noskov, S. Y.; Lamoureux, G.; Roux, B. Molecular Dynamics Study of Hydration in Ethanol−Water Mixtures Using a Polarizable Force Field. J. Phys. Chem. B 2005, 109, 6705-6713.
(75) Lamoureux, G.; Harder, E.; Vorobyov, I. V.; Roux, B.; MacKerell, A. D. A polarizable model of water for molecular dynamics simulations of biomolecules. Chem. Phys. Lett. 2006, 418, 245-249.
(76) Goloviznina, K.; Canongia Lopes, J. N.; Costa Gomes, M.; Pádua, A. A. H. Transferable, Polarizable Force Field for Ionic Liquids. J. Chem. Theory Comput. 2019, 15, 5858-5871.
(77) Goloviznina, K.; Gong, Z.; Padua, A. A. H. The CL&Pol polarizable force field for the simulation of ionic liquids and eutectic solvents. Wiley Interdiscip. Rev. Comput. Mol. Sci. 2022, 12.
(78) Breneman, C. M.; Wiberg, K. B. Determining atom-centered monopoles from molecular electrostatic potentials. The need for high sampling density in formamide conformational analysis. J. Comput. Chem. 1990, 11, 361-373.
(79) Frisch, M. J.; Trucks, G. W.; Schlegel, H. B.; Scuseria, G. E.; Robb, M. A.; Cheeseman, J. R.; Scalmani, G.; Barone, V.; Petersson, G. A.; Nakatsuji, H.; Li, X.; Caricato, M.; Marenich, A. V.; Bloino, J.; Janesko, B. G.; Gomperts, R.; Mennucci, B.; Hratchian, H. P.; Ortiz, J. V.; Izmaylov, A. F.; Sonnenberg, J. L.; Williams; Ding, F.; Lipparini, F.; Egidi, F.; Goings, J.; Peng, B.; Petrone, A.; Henderson, T.; Ranasinghe, D.; Zakrzewski, V. G.; Gao, J.; Rega, N.; Zheng, G.; Liang, W.; Hada, M.; Ehara, M.; Toyota, K.; Fukuda, R.; Hasegawa, J.; Ishida, M.; Nakajima, T.; Honda, Y.; Kitao, O.; Nakai, H.; Vreven, T.; Throssell, K.; Montgomery Jr., J. A.; Peralta, J. E.; Ogliaro, F.; Bearpark, M. J.; Heyd, J. J.; Brothers, E. N.; Kudin, K. N.; Staroverov, V. N.; Keith, T. A.; Kobayashi, R.; Normand, J.; Raghavachari, K.; Rendell, A. P.; Burant, J. C.; Iyengar, S. S.; Tomasi, J.; Cossi, M.; Millam, J. M.; Klene, M.; Adamo, C.; Cammi, R.; Ochterski, J. W.; Martin, R. L.; Morokuma, K.; Farkas, O.; Foresman, J. B.; Fox, D. J.: Gaussian 16 Rev. C.01. Wallingford, CT, 2016.
(80) Jorgensen, W. L.; Maxwell, D. S.; Tirado-Rives, J. Development and Testing of the OPLS All-Atom Force Field on Conformational Energetics and Properties of Organic Liquids. J. Am. Chem. Soc. 1996, 118, 11225-11236.
(81) Heid, E.; Szabadi, A.; Schröder, C. Quantum mechanical determination of atomic polarizabilities of ionic liquids. PCCP 2018, 20, 10992-10996.
(82) Brehm, M.; Kirchner, B. TRAVIS - A Free Analyzer and Visualizer for Monte Carlo and Molecular Dynamics Trajectories. J. Chem. Inf. Model. 2011, 51, 2007-2023.
(83) Brehm, M.; Thomas, M.; Gehrke, S.; Kirchner, B. TRAVIS—A free analyzer for trajectories from molecular simulation. Chem. Phys. 2020, 152, 164105.
(84) Humphrey, W.; Dalke, A.; Schulten, K. VMD: Visual molecular dynamics. J. Mol. Graph. 1996, 14, 33-38.